JGR Space Physics

RESEARCH ARTICLE
10.1029/2020JA028558

Investigation of the Interaction Between Magnetosheath Reconnection and Magnetopause Reconnection Driven by Oblique Interplanetary Tangential Discontinuity Using Three-Dimensional Global Hybrid Simulation

Zhifang Guo[1], **Yu Lin**[1], **and Xueyi Wang**[1]

[1]Physics Department, Auburn University, Auburn, AL, USA

Key Points:

- Magnetosheath reconnection due to interaction between an interplanetary directional tangential discontinuity (TD) and the bow shock/magnetosphere is investigated under the condition of an initially southward interplanetary magnetic field (IMF), and the results are compared with our previous cases with an initially northward IMF
- The existence and the structure of the magnetosheath reconnection are strongly dependent on the initial IMF direction, and the field rotation angle and half-width of the TD
- The magnetosheath reconnection co-exists with magnetopause reconnection, and the magnetosheath flux ropes can re-reconnect with the geomagnetic dipole field lines as they interact with the magnetopause

Correspondence to:
Z. Guo,
guozf@mail.iggcas.ac.cn

Citation:
Guo, Z., Lin, Y., & Wang, X. (2021). Investigation of the interaction between magnetosheath reconnection and magnetopause reconnection driven by oblique interplanetary tangential discontinuity using three-dimensional global hybrid simulation. *Journal of Geophysical Research: Space Physics*, *126*, e2020JA028558. https://doi.org/10.1029/2020JA028558

Received 11 AUG 2020
Accepted 15 DEC 2020

Abstract Magnetosheath reconnection due to the interaction of an interplanetary directional discontinuity with the bow shock and Earth's magnetosphere under an initially northward interplanetary magnetic field (IMF) has been investigated in previous simulations (e.g., Guo et al., 2018, https://doi.org/10.1029/2018ja025679). Under an initially southward IMF, the magnetosheath reconnection could interact with reconnection at the magnetopause. In this study, using three-dimensional (3D) global-scale hybrid simulations, we present cases with incoming tangential discontinuities (TDs) in an initially southward IMF, which possess various magnetic field rotation angles ($\Delta\Phi$) and half-width (w), to study the effects of pre-existing magnetopause reconnection on the formation of magnetosheath flux ropes, as well as the subsequent interaction between the magnetopause reconnection and magnetosheath reconnection, with downstreams of both Quasi-perpendicular (Q-$\perp$) and Quasi-parallel (Q-$\parallel$) shock examined. The initial IMF is assumed to be oblique, with a finite B_x and B_z, similar to that in Guo et al. (2018), https://doi.org/10.1029/2018ja025679 but with a southward $B_z < 0$. Compared with the cases with an initially northward IMF, magnetopause reconnection weakens the compression processes of the TD and leads to less frequent reconnection in the magnetosheath. The existence and the structure of magnetosheath reconnection are found to strongly depend on the parameters w and $\Delta\Phi$ of the TD. When interacting with the magnetopause reconnection, the magnetosheath flux ropes can re-reconnect with the geomagnetic dipole field lines, forming new structures of magnetopause flux ropes. The resulting evolution of flux rope configuration is illustrated.

1. Introduction

Discontinuous changes in magnetic field and plasma parameters are almost routinely observed in the solar wind (e.g., Archer et al., 2012; Burlaga, 1969, 1971; Kokubun et al., 1977; Lepping & Behannon, 1986; Ness, 1966; Nishida, 1978). These changes can be roughly characterized into two groups: interplanetary shocks and magnetohydrodynamic (MHD) discontinuities. Among them, tangential discontinuities (TDs) and rotational discontinuities (RDs) are most frequently present (e.g., Burlaga, 1969, 1971; Lepping & Behannon, 1986). TDs can be considered as a current sheet, in which magnetic field direction is parallel to the surface on both sides of the TDs, and thus the normal component of the field $B_n = 0$. TDs do not propagate in the plasma frame, but are convected by the solar wind plasma flows. Across the TDs, the plasma density and magnetic field strength can vary, while the total pressure is balanced. RDs can be considered as large-amplitude Alfven waves with a finite $B_n \neq 0$, which that propagate in the plasma frame with the normal Alfven speed, V_{An}.

In the solar wind, discontinuities carrying a magnetic field direction variation are more frequently observed than those with a significant field magnitude change (Burlaga, 1968; Burlaga & Ness, 1968). This special class of discontinuities are called directional discontinuities (DDs), across which only the magnetic field direction changes, while the magnetic field strength and plasma density remain constant. The observed DDs in the solar wind include directional tangential discontinuities or rotational discontinuities (e.g., Behannon et al., 1981; Burlaga et al., 1977; Lepping & Behannon, 1986; Ness, 1966). Although a DD carries only a magnetic field direction change, the consequence of its interaction with the bow shock is far more complicated than a simple turning of the magnetic field direction. The interaction is found to be closely associated with the formation of hot flow anomalies (HFAs) (e.g., Eastwood et al., 2008; Lin, 1977, 2002;

Maynard et al., 2002; Omidi et al., 2014; S. Wang et al., 2013), foreshock bubbles (FBs; Liu et al., 2015; Omidi et al., 2010), foreshock cavities (Lin, 2003; Lin & Wang, 2005; Omidi et al., 2013), and the generation of Ultra low frequency (ULF) waves (Le & Russell, 1992). Numerous studies have suggested that HFAs are related to magnetosheath flow deflections due to the interaction of an interplanetary directional TD with the bow shock (e.g., Lin, 2003; Thomson et al., 1993; Schwartz et al., 1995, 2000; D. G. Sibeck et al., 1999, 2000). On the other hand, observational and simulation studies have shown that compression of a solar wind directional TD can trigger magnetic reconnection in the magnetosheath when the current sheet passes through the bow shock (Hasegawa et al., 2010; Lin, 1997; Omidi et al., 2009; T. D. Phan et al., 2007, 2011). Magnetosheath reconnection downstream of the bow shock due to the interaction between a directional TD and the bow shock has been investigated by performing two-dimensional (2D; Omidi et al., 2009) and three-dimensional (3D; Guo et al., 2018; Pang et al., 2010) hybrid simulations.

Although the magnetic field direction of DDs can change arbitrary, DDs dominated by a change in the sign of the B_z component of the interplanetary magnetic field (IMF) may be more geoeffective. According to the sign of the B_z component of the IMF, DDs in the solar wind can have a southward-to-northward (S-N) turning of IMF or northward-to-southward (N-S) turning of IMF. Once the interplanetary DD passes through the bow shock, its subsequent interaction with the Earth's magnetosphere is closely related to the B_z directions across the DDs. While a southward turning of IMF may interact with the magnetosphere in the way that causes magnetic reconnection at the dayside magnetopause and trigger magnetospheric substorms, a northward turning of IMF may also trigger magnetospheric substorms (Hsu & McPherron, 2003; Lyons et al., 1977; Thomsen et al., 2003), leading to the transfer of magnetic flux and energy from the solar wind to the Earth's magnetosphere (Dungey, 1961; Guo et al., 2020; Hasegawa et al., 2010; Paschmann et al., 1979; R. Wang et al., 2017).

Previously, interaction between the dayside bow shock-magnetosphere system and an interplanetary directional TD with a southward turning IMF has been simulated by using 3D (Guo et al., 2018; Pang et al., 2010) global hybrid models, while the initial IMF (on the earthward side of the TD) points northward. A two-step compression process of the TD has been identified, including the shock compression at the bow shock and the convective compression in the magnetosheath. In our previous 3D global hybrid simulation for a TD with an N-S turning of IMF (Guo et al., 2018), the generation of magnetosheath reconnection downstream of both Q-$\perp$ and quasi-parallel (Q-$\parallel$) shocks is found.

In the above case with an initially northward IMF, a magnetic barrier exists in front of the magnetopause due to the pile up of the northward magnetic field (Crooker et al., 1979; Paschmann et al., 1993; T. Phan et al., 1994; Pudovkin, 1987; Samsonov et al., 2017). The field pileup helps to compress the incoming TD in the stage of the convective compression of the transmitted discontinuity in the magnetosheath (Guo et al., 2018; Pang et al., 2010). Nevertheless, if the IMF direction change is switched to S-N across the incoming TD, so the IMF is initially southward, reconnection can be triggered at the dayside magnetopause before the TD arrives at the bow shock. Under such a precondition, the magnetic flux in front of the incoming TD would be continuously removed by the magnetopause reconnection (T. Phan et al., 1994). As a result, the magnetopause reconnection on the earthward side of the TD may affect the generation and structure of the magnetosheath reconnection/flux ropes inside the TD. Moreover, the flux ropes generated in the magnetosheath may re-reconnect with the magnetopause field lines.

To fully understand the effects of the B_z component of IMF in a directional TD on the magnetosheath reconnection and the subsequent impacts to the magnetopause, in this paper, we extend our previous 3D global-scale hybrid simulations of the TD-bow shock-magnetosphere interaction to cases in which the TD possesses an S-N turning of IMF. We first investigate the generation, evolution, and global structure of magnetosheath flux ropes downstream of both Q-$\perp$ and Q-$\parallel$ shocks. Under similar conditions of the initial IMF B_z, cases with various magnetic field rotation angles and initial half-widths of the directional TDs will be studied. Then, interaction of the generated magnetosheath flux ropes with the magnetopause field lines/flux ropes is investigated. Results of this study will also be compared with our previous simulations (Guo et al., 2018) with an N-S change of IMF across the directional TD.

This study is organized as follows. Section 2 describes our simulation model. The simulation results are presented in Section 3. Finally, summary and discussion are given in Section 4.

2. Simulation Model

A 3D global-scale hybrid simulation (Lin & Wang, 2005) is used, similar to our previous study for the generation of the magnetosheath reconnection in the interaction between an interplanetary TD and the dayside magnetosphere (Guo et al., 2018), in which the ions are treated as discrete particles and the electrons are considered to be a massless fluid. In our self-consistent scheme, the ions are accelerated by their equation of motion, the magnetic field is advanced by Faraday's law, and the electric field is determined by the electron momentum equation. A current-dependent resistivity is included in the simulation. The 3D simulation is carried out in the spherical coordinates system. A total grid of $n_r \times n_\theta \times n_\phi = 220 \times 114 \times 150$ is used, which consists of the radial distance r, the zenith angle θ measured from the positive GSM z-axis, and the azimuthal angle φ from the negative GSM y-axis. The earth is located at the origin. The simulation domain is a region with $3.5R_E \le r \le 23R_E$, $0° \le \theta \le 180°$, and $20° \le \varphi \le 160°$. Nonuniform grids in the r direction are exploited, with a higher resolution of $\Delta r = 0.05R_E$ for $r \in [9R_E, 14R_E]$, throughout the bow shock, magnetosheath, and magnetopause regions. In the case presented, the solar wind ion gyrofrequency Ω_{i0} is set as $0.958s^{-1}$, corresponding to IMF $B_0 = 10nT$. For a typical solar wind density of 6/c.c., the values of the solar wind ion inertial length d_{i0} is $0.0148R_E$, where $d_{i0} = c / \omega_{pi0}$, ω_{pi0} is the ion plasma frequency and c is the light speed. The solar wind ion inertial length used in the simulation is chosen to be $0.1R_E$, a factor of ~6–7 lager than the realistic values.

In this simulation, the magnetic field B and ion number density N are scaled by the unperturbed solar wind IMF B_0 and density n_0, respectively. The time t is expressed by the inverse of ion gyro-frequency Ω_{i0}^{-1} ($\Omega_{i0} = eB_0 / m_i$) in the solar wind, e is the electron charge, m_i is the ion mass; the plasma flow velocity V by the solar wind Alfvén speed V_{A0}, where $V_{A0} = B_0 / \sqrt{\mu_0 m_i n_0}$; the thermal pressure by $n_0 m_i V_{A0}^2$; and the electric field by V_{A0B0}. To illustrate the simulation results on the spatial scales of the Earth's magnetosphere, the length is plotted in units of the Earth radius (R_E), and the GSM coordinate is used. The solar wind flows with $V_{0x} = -500$ km/s carrying the IMF toward the Earth along the $-x$ direction, with an Alfvén Mach number $M_A = 5.6$, from the inflow boundary at $r = 23R_E$. Outflow boundary conditions are applied at $\theta = 0^\circ$ and 180°, corresponding to $x = 0$. The inner boundary at $r = 3.5R_E$ is treated as an ideal conducting boundary, and an additional cold ion fluid is used to model the inner magnetosphere at $r \le 6.5R_E$. The particle number per cell is about 150–600 for the interested regions of the magnetosheath and magnetopause.

The bow shock and the magnetopause are first formed by the self-consistent interaction of the convection of the solar wind with the geomagnetic field. Then, an interplanetary TD is allowed to propagate into the domain toward the Earth. In this study, we are only interested in cases of a directional TD, which possesses various magnetic field rotational angles and initial half-widths. We assume that the tangential magnetic field direction and initial half-width of the directional TD can change arbitrarily across the TD, but the plasma density, total pressure, and field strength do not change. The initial IMF is assumed to be oblique, with $\left(B_x, B_y, B_z\right) = \left(0.5, 0.0, -0.866\right) B_0$ and thus a southward B_z.

Initially, the front of the directional TD is assumed to be at a distance corresponding to $x = 36R_E$ at $z = 0R_E$, outside the simulation domain (i.e., the TD is set to convect, with the solar wind speed, into the domain at $t \sim 14.0\Omega_{i0}^{-1}$.). The TD moves toward the Earth with the solar wind flows. The normal magnetic field component of the directional TD is $B_n = 0$, and thus the TD front makes an angle of 30° relative to z direction. The normal direction of the TD is oblique to the x-axis, with $n = \left(-0.866, 0, -0.5\right)$. More detailed description of the model and the directional TD can be found in Guo et al. (2018).

Let w be the half-width of the initial TD, and $\Delta\Phi$ denote the rotational angle of the tangential magnetic field across the TD. The IMF B_z changes from southward to northward (i.e., S-N) across the TD, and the TD possesses a circularly polarized magnetic field. In order to understand the generation, structure, and dynamic evolution of the magnetosheath reconnection downstream of the shock, five cases are presented in this paper for TDs with an S-N field variation, with various $\Delta\Phi = 90°$ to 180° and $w = 5d_{i0}$ to $30d_{i0}$, as listed in Table 1.

Table 1
Simulation Cases Presented in This Study, With the Various Rotation Angles $\Delta\Phi$ and Initial Half-Width w of the Transmitted TD in the Solar wind

Case	$\Delta\Phi(^\circ)$	$w(d_{i0})$
1	180	10
2	150	10
3	120	10
4	180	5
5	180	30

Note: that d_i0 is the ion inertial length in the solar wind.

3. Simulations Results

As described in Section 2, the initial IMF in all five cases is assumed to be $(B_x, B_y, B_z) = (0.5, 0.0, -0.866)B_0$, with a southward B_z in the simulation domain. At $t = 0$, the directional TD front is located at a distance corresponding to $x = 36.0R_E$ at $z = 0R_E$, outside the simulation domain. The TD convects in the $-x$ direction toward the Earth with the solar wind flows. Different from our previous simulations by Guo et al. (2018), in which the initial IMF is northward, magnetic reconnection takes place at the dayside magnetopause before the impacts of the TD. Outside the magnetopause, magnetosheath reconnection is triggered by interaction between the TD and the bow shock/magnetosheath, forming long flux ropes in the dawn-dusk direction outside the magnetopause. As the magnetosheath flux ropes reach the magnetopause, re-reconnection between the reconnected magnetosheath flux ropes and the geomagnetic dipole field lines takes place, changing the structure of magnetopause flux ropes. The details of the physical processes are presented in the following.

3.1. Magnetopause Reconnection Associated With the Initial IMF Conditions

In the early stage of the simulation runs, the bow shock, magnetosheath, and magnetopause form in a self-consistent manner under the initial IMF conditions. Magnetic reconnection is triggered at the magnetopause under the oblique IMF. Flux ropes are generated, and the structure of the reconnected magnetic field lines is approximately symmetric about the noon meridian plane under the initial IMF with $B_y = 0$.

Figure 1 shows the magnetic field line configuration at the magnetopause in a zoom-in view at $t = 40.0\Omega_{i0}^{-1}$. The contours in the figure display the magnetic field strength in the noon meridian plane. The magnetosheath field lines are marked by the orange lines, and the arrows indicate the directions of the local magnetic field. Lines of black color indicate the reconnected field lines at the magnetopause, which connect between the IMF and the Earth's dipole field (to the north and south pole). The central position of the

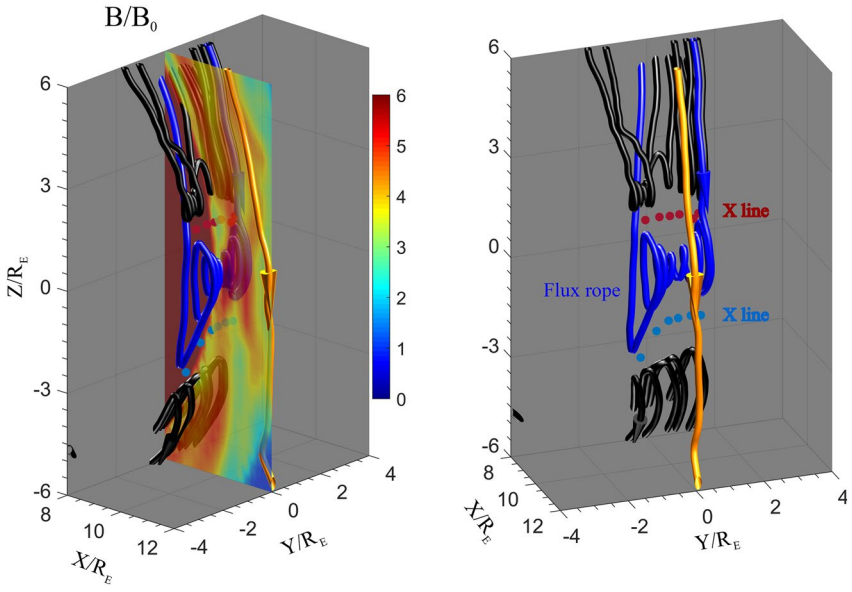

Figure 1. Magnetopause reconnection prior to the TD arrival. Magnetic field line configuration in a global view obtained in case 1 at $t = 40.0\Omega_{i0}^{-1}$. The magnetosheath field lines are in orange. Field lines in other colors are the reconnected field lines at the magnetopause. Contours in the noon meridian plane show the magnetic field strength. The red and blue dashed lines denote two neighboring X lines. TD, tangential discontinuities.

magnetopause can be identified by the sharp gradient of the magnetic field strength around $x \approx 10.0R_E$ through the subsolar point. Two X lines are denoted by blue and red dashed lines in Figure 1, whose lengths are about $2-3R_E$ in the dawn-dusk direction, which are identified by the magnetic field line configuration obtained in the simulation (Guo et al., 2018; Tan et al., 2012). The magnetopause flux ropes are formed between the two neighboring X lines, shown by the blue field lines, corresponding to multiple X line reconnection (MXR; Fu & Lee, 1985; Tan et al., 2012). As these magnetopause flux ropes move poleward with the magnetosheath flows, new flux ropes are formed near the original location, and the process repeats in time, as discussed in work of Guo et al. (2020). In fact, there are four types of flux ropes in the magnetopause reconnection. The field line configuration of the four types of the magnetopause flux ropes will be elaborated in Section 3.4. The magnetopause reconnection is present until the incoming TD is transmitted through and leaves the dayside magnetopause.

3.2. Magnetosheath Reconnection due to the Incoming TD

3.2.1. Downstream of the Q-⊥ Shock

Now, we present the results of the interaction between the incoming TD and the Q-⊥ shock/magnetosphere, starting from case 1, in which the field rotational angle and the initial half-width of the TD are $\Delta\Phi = 180°$ and $w = 10d_{i0}$, respectively. To illustrate the time evolution of the TD, Figure 2 displays the magnetic field line configuration for case 1. Three colors of the magnetic field lines are shown, with the blue ones being the reconnected field lines (flux ropes) at the magnetopause, the orange field lines marking the open interplanetary field lines outside the magnetopause, and the green ones representing the field lines of the TD. The colored sphere at the origin represents the Earth. Recall that the initial IMF is $\left(B_x, B_y, B_z\right) = \left(0.5, 0.0, -0.866\right)B_0$ on the earthward side of the incoming TD, marked by the orange field lines in Figure 2a. The TD starts to convect into the outer boundary at $t \approx 14.0\Omega_{i0}^{-1}$. The magnetic field in the simulation domain changes in response to the arrival of the TD at each specific point, as described by equations 7 and 8 in Guo et al. (2018). A field line around the TD is denoted by the green line in Figure 2a.

In the simulation, the bow shock is well developed at $t \approx 25.0\Omega_{i0}^{-1}$ in front of the magnetopause. As shown in Figure 2b, the TD has already convected into the simulation domain outside the bow shock at $t = 30.0\Omega_{i0}^{-1}$. At $t \approx 35.0\Omega_{i0}^{-1}$, the TD interacts with part of the Q-⊥ shock, as seen from the perturbed green field line in Figure 2c. It is noted that no magnetic reconnection occurs inside the TD before it interacts with the bow shock. As the TD passes through the bow shock, it is dragged tailward by the magnetosheath flows, forming a paraboloidal-shaped structure. At $t = 60.0\Omega_{i0}^{-1}$, magnetic flux ropes have already formed by 3D patchy magnetic reconnection downstream of the Q-⊥ bow shock, marked by the orange helical field lines in Figure 2d. The transmitted TD is narrowed by the shock compression and the convective compression process, which are discussed in work of Guo et al. (2018). In the dawn-dusk direction, the length of the magnetosheath flux ropes is $\sim 24.0R_E$, which is much longer than that of the magnetopause flux ropes ($\sim 3.0R_E$) in Figures 2c–2d.

After the reconnection flux ropes are formed inside the TDs downstream of the Q-⊥ shock, they propagate northward and tailward with the magnetosheath plasma flows. When these magnetosheath flux ropes reach and interact with the magnetopause, magnetic reconnection occurs between the magnetosheath flux ropes and the magnetopause field lines, undergoing a "re-reconnection" process. To illustration the time evolution of the magnetosheath flux ropes, Figures 3a–3f highlight the field line configuration of the magnetosheath flux ropes downstream of the Q-⊥ shock in a 3D global view at $t = 50.0\Omega_{i0}^{-1}$, $60.0\Omega_{i0}^{-1}$, and $70.0\Omega_{i0}^{-1}$, obtained in case 1. The magnetic field line configurations at the magnetopause in a zoom-in view at $t = 50.0\Omega_{i0}^{-1}$ and $70.0\Omega_{i0}^{-1}$ are shown in Figures 3g and 3h, respectively. The contours in Figures 3a–3c display the magnetic field strength in the noon meridian plane. The orange field lines are the magnetosheath flux ropes inside the transmitted TD, the blue field lines represent the flux ropes at the magnetopause, and the red ones mark the re-reconnected field lines between the magnetosheath flux ropes and magnetopause field lines. Six magnetosheath flux ropes downstream of the Q-⊥ shock are highlighted in Figures 3d–3f, as marked by "A," "B," "C," "D," "E," and "F." In Figures 3a and 3d, it is clearly seen that five magnetosheath flux ropes have already formed at $t = 50.0\Omega_{i0}^{-1}$, as marked by "A," "B," "C," "D," and "E." These magnetosheath flux ropes

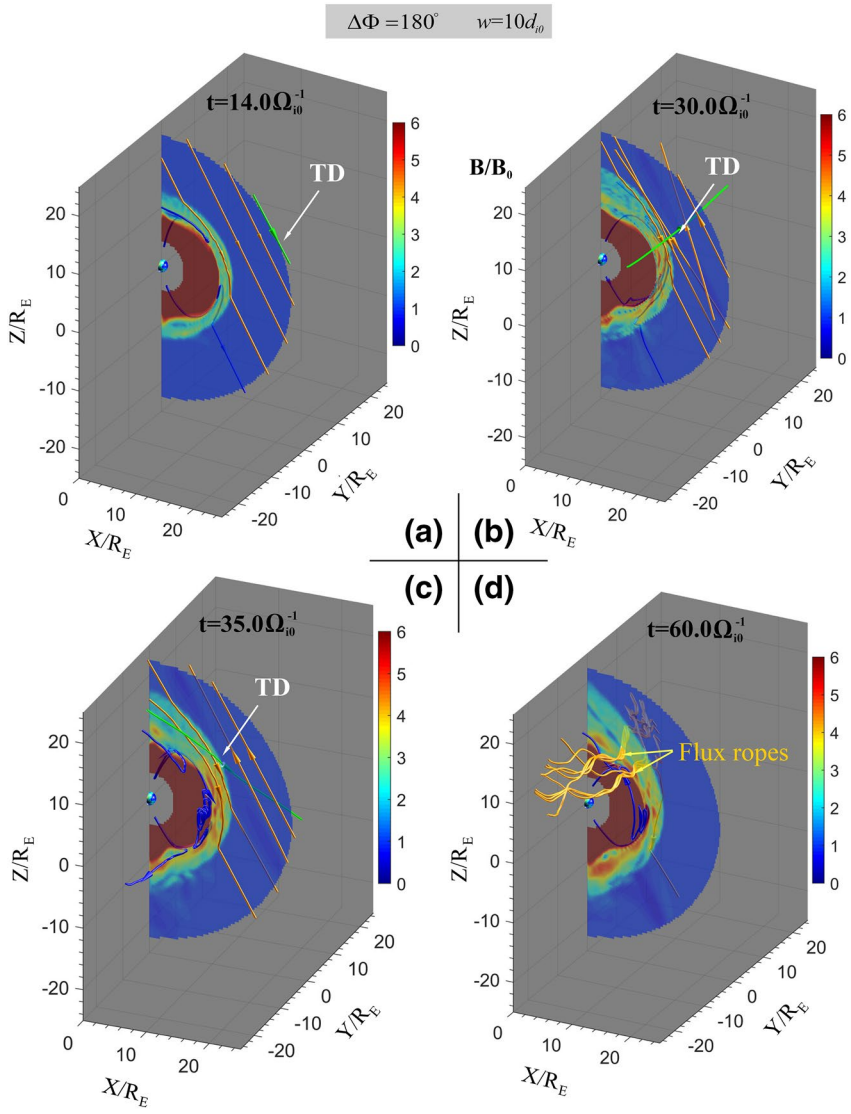

Figure 2. Interaction of the TD with the Q-⊥ shock and magnetosheath. Contours of the magnetic field strength in the noon meridian plane at (a) $t = 14.0\,\Omega_{i0}^{-1}$, (b) $30.0\Omega_{i0}^{-1}$, (c) $35.0\Omega_{i0}^{-1}$, and (d) $60.0\Omega_{i0}^{-1}$ obtained in case 1. The blue field lines are the reconnected field lines at the magnetopause, the orange ones denote the interplanetary field lines around the transmitted TD outside the magnetopause, and the green field lines represent the field lines of the TD. TD, tangential discontinuities.

subsequently propagate poleward with the magnetosheath flows, as sketched by the black arrows and also shown in our previous work (Figure 7, Guo et al., 2018). At $t = 60.0\Omega_{i0}^{-1}$, flux rope "A" has moved out of the tail-side boundary, while a new flux rope "F" has formed, as shown in Figures 3b and 3e. At $t = 70.0\Omega_{i0}^{-1}$, flux ropes "B" and "C" have left the tail-side boundary. In the meantime, flux rope "F" has reached and is interacting with the magnetopause, resulting in a newly reformed magnetopause flux ropes by re-reconnection, as shown by the red field line in Figures 3c and 3f. The length in the dawn-dusk direction of the newly reformed magnetopause flux ropes is much longer than that of original magnetopause flux ropes, as shown in Figures 3g and 3h. The details of the re-reconnection process will be further elaborated in Section 3.3.

The structures of the magnetosheath flux ropes are different for incoming TDs with different rotation angles $\Delta\Phi$ and initial half-width w. To discuss the effects of rotation angles $\Delta\Phi$ on the generation of magnetosheath flux ropes, assuming $w = 10d_{i0}$, Figures 4a–4c display the field line configuration inside the TD obtained

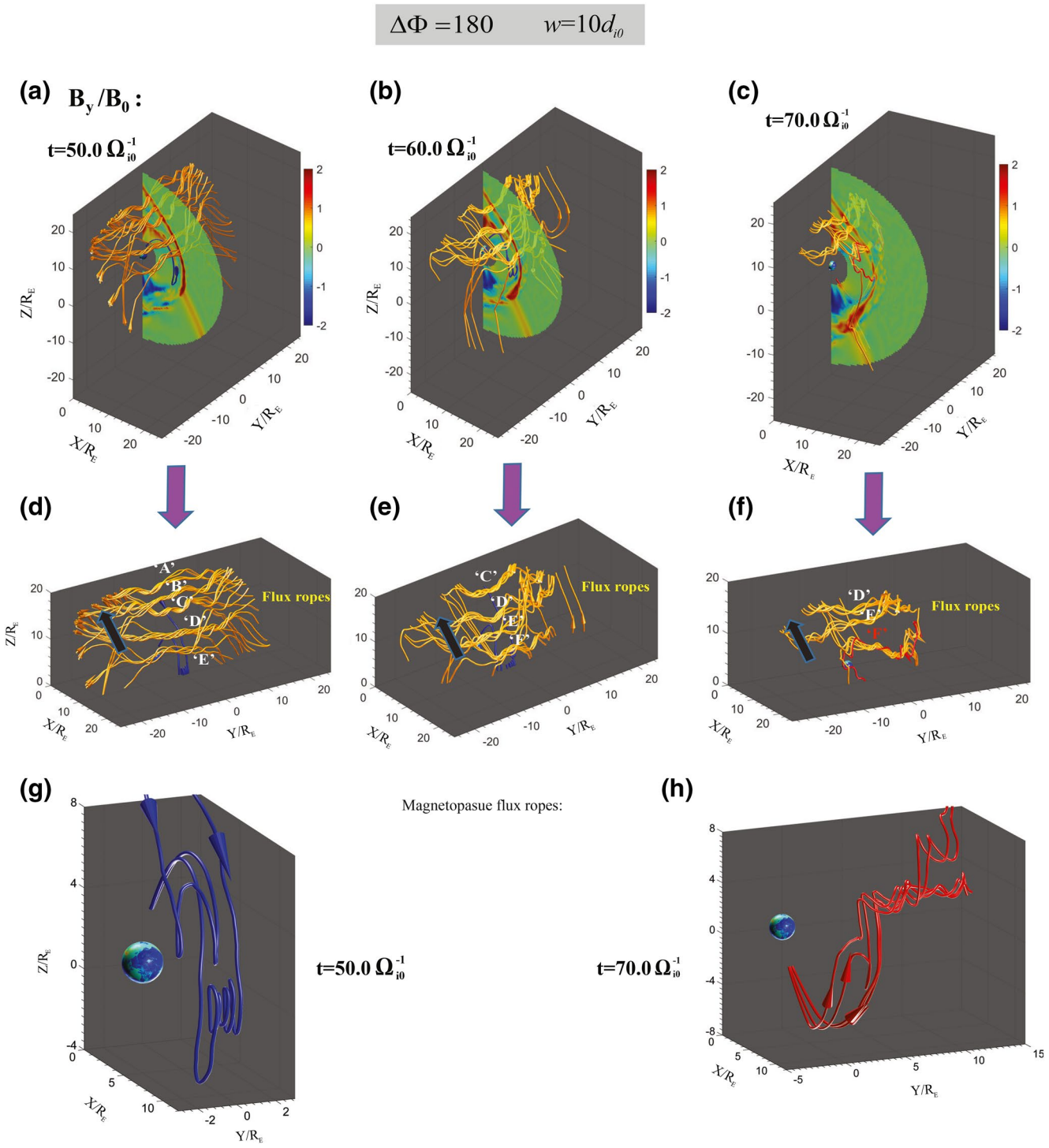

Figure 3. Time evolution of the magnetosheath and magnetopause flux ropes. (Top) Contours of the B_y component in the noon meridian plane and (middle) typical magnetic field lines in a zoom-in view downstream of the Q-⊥ shock obtained at (a and d) $t = 50.0\Omega_{i0}^{-1}$, (b and e) $60.0\Omega_{i0}^{-1}$, and (c and f) $70.0\Omega_{i0}^{-1}$. The magnetic field line configurations in the bottom row depict the magnetopause flux ropes before and after re-reconnection between the magnetosheath flux rope and the magnetopause field lines. The orange field lines denote the magnetosheath magnetic flux ropes, the blue field lines are the reconnected magnetopause field lines, and the red one marks the re-reconnection field lines. Bundles of the y-component fluxes are marked by "A," "B," "C," "D", "E,", and "F." The black arrows indicate the propagation directions of these magnetosheath flux ropes.

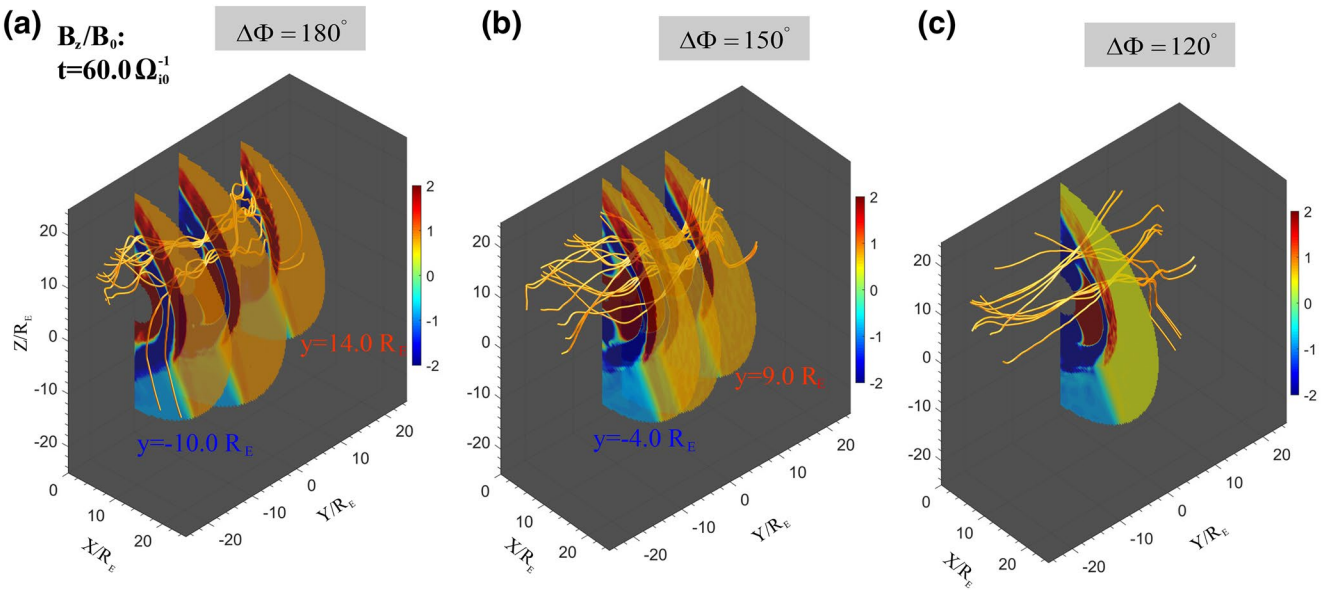

Figure 4. Effects of ΔΦ on the generation of magnetosheath flux ropes. Magnetic field line configuration in a global view inside the TD downstream of the Q-⊥ shock obtained at $t = 60.0\Omega_{i0}^{-1}$, in cases with (a) $\Delta\Phi = 180°$ (case 1), (b) 150° (case 2), and (c) 120° (case 3), assuming $w = 10d_{i0}$. Contours in the noon meridian plane show the B_z component. The orange field lines are the field lines inside the TD. TD, tangential discontinuities.

at $t = 60.0\Omega_{i0}^{-1}$, for $\Delta\Phi = 180°$ (case 1, Figure 4a), 150° (case 2, Figure 4b), and 120° (case 3, Figure 4c). The contours in this figure show the component B_z in various planes parallel to the noon meridian plane. The orange lines denote the field lines inside the TD downstream of the Q-⊥ shock. As shown in Figure 4a, magnetic flux ropes with length of $\sim 24.0R_E$ in the dawn-dusk direction, from $y = -10.0R_E$ to $14.0R_E$, are present in case 1 with $\Delta\Phi = 180°$. When ΔΦ decreases to 150°, the flux rope length has decreased to $\sim 13.0R_E$, within the region from $y = -4.0R_E$ to $9.0R_E$, as shown in Figure 4b. Overall, longer flux ropes are found in cases with a larger rotation angle ΔΦ. In addition, the magnetosheath flux ropes in case 1 were initially formed at $t \sim 43.0\Omega_{i0}^{-1}$, which is earlier than that in case 2 with a similar ΔΦ (at $t \sim 48.0\Omega_{i0}^{-1}$). For case 3 in which ΔΦ is further reduced to 120°, however, no magnetosheath flux ropes are seen in Figure 4c, and no flux ropes can be found in the entire run.

Next, we investigate effects of the initial half-width w of TD on the structures of the magnetic flux ropes downstream of the Q-⊥ shock, assuming $\Delta\Phi = 180°$. Figures 5a–5d show the component B_y in the noon meridian plane for cases with $w = 10d_{i0}$ (case 1, Figure 5a), $5d_{i0}$ (case 4, Figure 5b), and $30d_{i0}$ (case 5, Figure 5c) obtained at $t = 60.0\Omega_{i0}^{-1}$. The orange lines in the figure are the field lines inside the TD. In Figure 5a, the red line denotes the magnetic field line around the bow shock, and the black arrow indicates the normal direction of the bow shock. At $z = -3.5R_E$ around the bow shock, the shock normal angle $\theta_{Bn} = 45°$. The region with $\theta_{Bn} > 45°$ on the bow shock is located at $z > -3.5R_E$, corresponding to the Q-⊥ shock. In case 4 with $w = 5d_{i0}$ and case 1 with $w = 10d_{i0}$, magnetosheath flux ropes are formed downstream of the Q-⊥ shock, as seen from the orange field lines in Figures 5a and 5b. In case 4 with a thinner initial width ($5d_{i0}$), the magnetosheath flux ropes were formed at $t \sim 39.0\Omega_{i0}^{-1}$, earlier than that in case 1 ($t \sim 43.0\Omega_{i0}^{-1}$). Moreover, the length of the flux ropes in case 4 ($\sim 30R_E$) is longer than that in case 1 ($\sim 24R_E$). In case 5 with a much wider $w = 30d_{i0}$, however, no reconnection flux ropes can be found, as shown in Figure 5c.

3.2.2. Downstream of the Q-|| Shock

Due to the difference in magnetic field geometries around the Q-|| shock and Q-⊥ shock and the weaker compressibility at the Q-|| shock, magnetic reconnection is less frequently present in the TD downstream of the Q-|| shock than the Q-⊥ shock. Figures 6a and 6b display the magnetic field line configuration inside the TD downstream of the Q-|| shock for $w = 10d_{i0}$ (case 1) and $w = 5d_{i0}$ (case 4) obtained at $t = 60.0\Omega_{i0}^{-1}$, assuming $\Delta\Phi = 180°$, with the contours showing the B_y component in the noon meridian plane. Again,

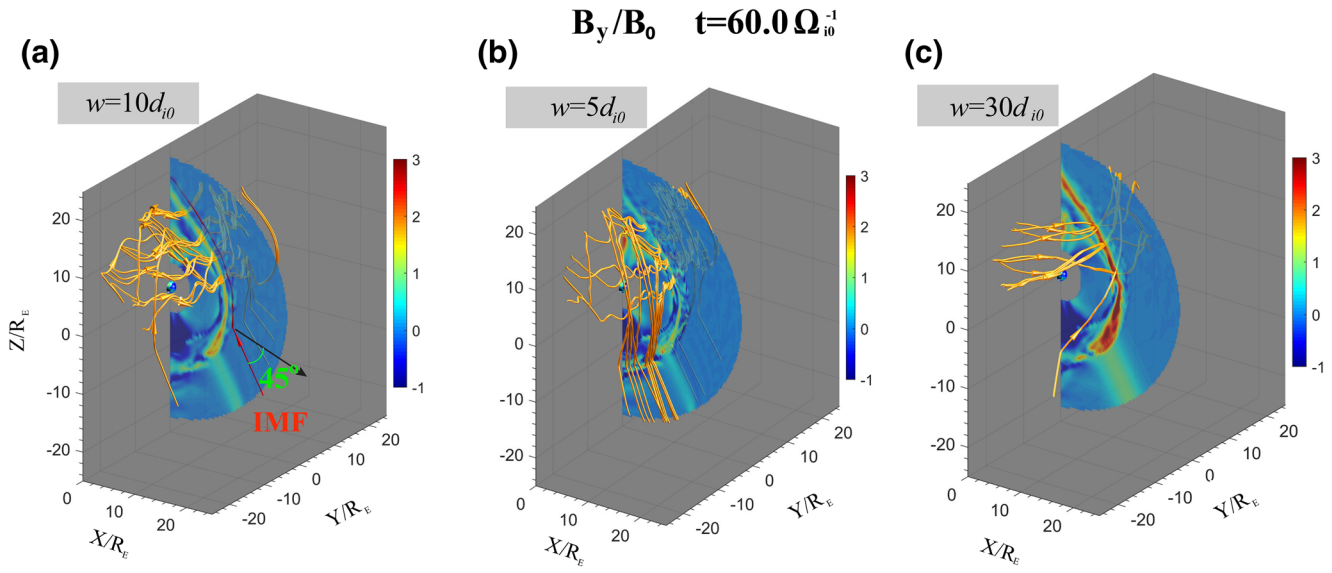

Figure 5. Effects of the TD width on the structure of flux ropes downstream of the Q-⊥ shock. Contours of the B_y component in the noon meridian plane with the initial half-width (a) $w = 10d_{i0}$ (case 1), (b) $5d_{i0}$ (case 4), and (c) $30d_{i0}$ (case 5) obtained at $t = 60.0\Omega_{i0}^{-1}$. The orange field lines are the field lines inside the TD downstream of the Q-⊥ shock, and the red line denotes the magnetic field line where the normal shock angle $\theta_{Bn} = 45°$ around the bow shock. TD, tangential discontinuities.

the orange lines are the field lines inside the TD downstream of the Q-∥ shock. It is clearly shown that no magnetosheath flux ropes exist downstream of the Q-|| shock in case 1 with $w = 10d_{i0}$ (Figure 6a). But flux ropes with helical field line configuration are present near the magnetopause downstream of the Q-|| bow shock in case 4 with a narrower $w = 5d_{i0}$. The length of the flux ropes is ~$6.5R_E$, within the region from $y = -3.0R_E$ to $3.5R_E$, as shown in Figure 6b. Our simulation indicates that compared with the results

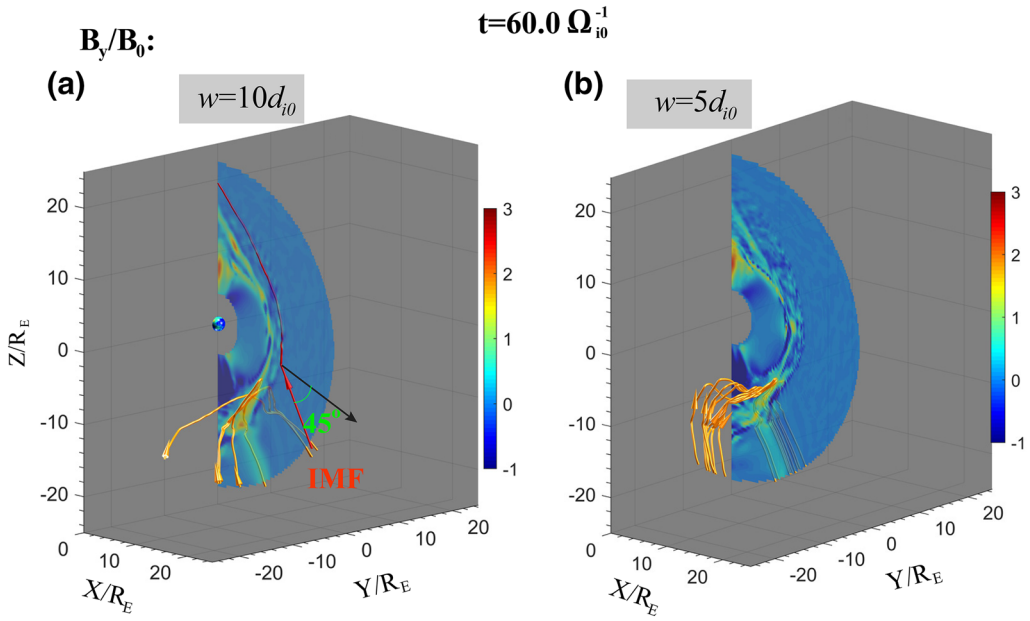

Figure 6. Effects of the TD width on the structure of flux ropes downstream of the Q-∥ shock. Magnetic field line configuration inside the TD downstream of the Q-|| shock in cases with the initial half-width (a) $w = 10d_{i0}$ (case 1) and (b) $5d_{i0}$ (case 4) obtained at $t = 60.0\Omega_{i0}^{-1}$, assuming $\Delta\Phi = 180°$. Contours in the noon meridian plane show the B_y component. The field lines in orange are the field lines inside the TD downstream of the Q-|| shock. TD, tangential discontinuities.

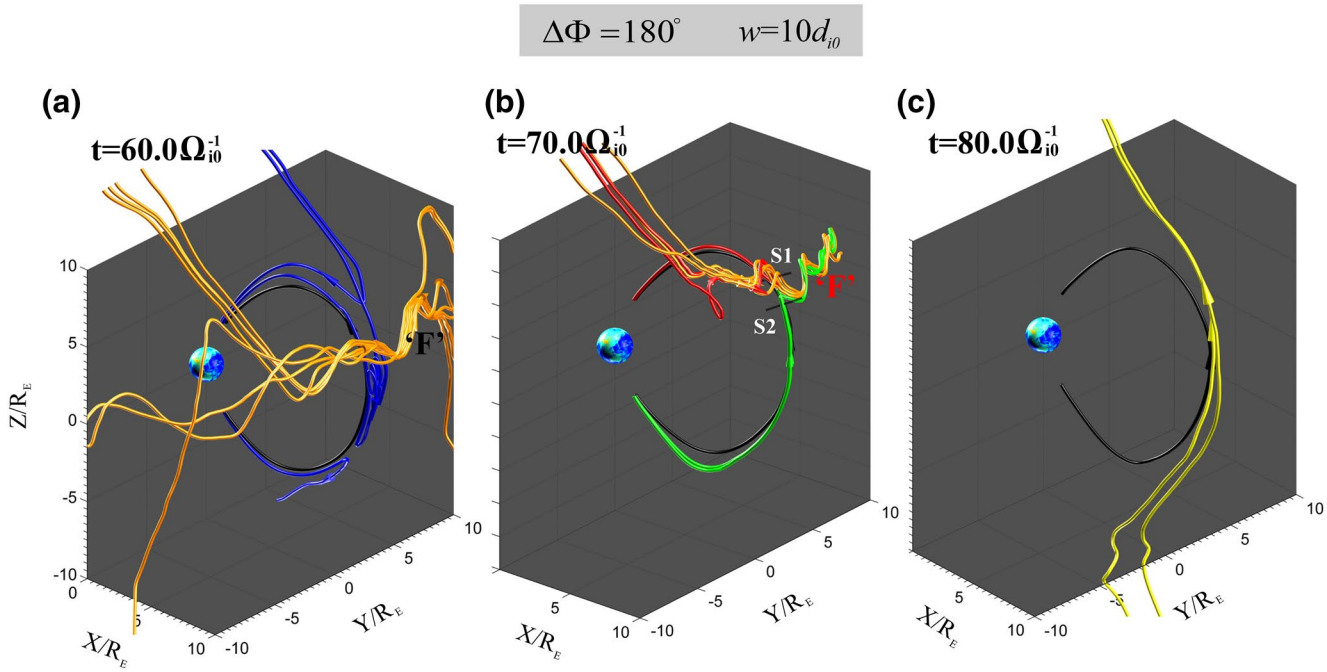

Figure 7. Interaction of magnetosheath flux ropes with the magnetopause. Magntic field line configuration at (a) $t = 60.0\Omega_{i0}^{-1}$, (b) $70.0\Omega_{i0}^{-1}$, and (c) $80.0\Omega_{i0}^{-1}$ around the magnetopause. The blue field lines are the reconnected magnetopause field lines, the field lines in orange denote the magnetic flux ropes inside the TD, the field line in yellow marks the northward IMF line, and the red and the green field lines are the re-reconnection field lines. The two paths, marked by S1 (northward of the re-reconnection X point) and S2 (southward of the re-reconnection X point), are through the magnetopause re-reconnection current layers in Figure 4b. TD, tangential discontinuities.

downstream of the Q-⊥ shock, a much thinner current sheet is required for reconnection to be triggered by compression of the TD downstream of the Q-∥ shock.

3.2.3. Comparison With the N-S Cases of Guo et al. (2018)

In all the five cases shown above, in which the initial IMF B_z is southward, magnetopause reconnection is present until the incoming TD passes through the dayside magnetopause. The magnetopause reconnection plays an important role in the evolution of the transmitted TDs, and on the generation of the magentosheath flux ropes. In the following, we compare our present simulation with the previous work of Guo et al. (2018), in which the IMF change from N to S and thus no reconnection occurs at the magnetopause before the arrival of TD.

Under the same conditions of w and ΔΦ, magnetoshath reconnection occurs more frequently in the N-S cases than S-N cases. For example, in the case with $w = 10d_{i0}$ and $\Delta\Phi = 120°$, reconnection flux ropes are present (Guo et al., 2018), while no magnetosheath flux ropes are formed in the present S-N case (case 3). For the case with a wider $w = 30d_{i0}$ and $\Delta\Phi = 180°$, magnetosheath flux ropes are seen in the N-S case (Guo et al., 2018). Nevertheless, no reconnection flux ropes are present in the N-S case (case 5). In addition, in the case with $w = 10d_{i0}$ and $\Delta\Phi = 180°$, reconnection flux ropes are formed in both the Q-⊥ and Q-|| shocks in the N-S case (Guo et al., 2018), while in the S-N case they only form in the Q-⊥ shock (case 1). Moreover, the stay time of the transmitted TD in the magnetosheath is shorter in the S-N case than in the N-S case. For example, in the case with $w = 30d_{i0}$ and $\Delta\Phi = 180°$, the transmitted TD interacts with the Q-⊥ shock at $t \approx 35.0\Omega_{i0}^{-1}$ and passes through the tail-side boundary at $t \approx 80.0\Omega_{i0}^{-1}$ in the S-N case (case 5) shown above, but the TD stays in the dayside domain until $t \approx 95.0\Omega_{i0}^{-1}$ in the N-S case (Guo et al., 2018). Our results indicate that the transmitted TD convects more slowly in the magnetosheath in the N-S case than the S-N case due to the much stronger magnetic flux pileup, and a long enough stay time of the TD in the magnetosheath is required for reconnection to be trigger by convective compression of the TD.

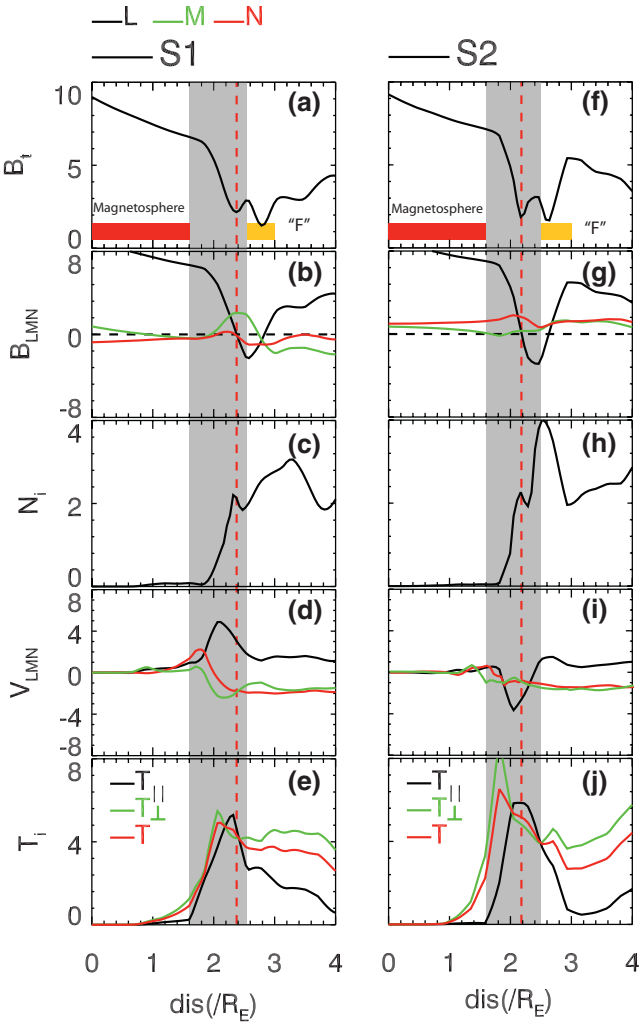

Figure 8. Structure of the magnetic field and plasma quantities around the re-reconnection X point. Spatial profiles (a and f) the field strength B, (b and g) field components B_L (black), B_M (green), and B_N (red) in the LMN coordinate system, (c and h) ion number density N_i (d and i) ion bulk flows in the LMN coordinates, and (e and j) ion temperatures $T_{\|}$ (black), $T_{\perp}$ (green) and the total ion temperature T (red) in the outbound direction along path S1 (left) and S2 (right) in Figure 4. The locations of the center of the reconnection current layer are denoted by a vertical dotted red lines. The shaded region in the figure represents the magnetopause reconnection current layer.

In work of Guo et al. (2018) with an N-S IMF change, magnetopause reconnection is only found when the southward IMF on the sunward side of the TD interacts with the northward geomagnetic field, and thus unlike the S-N cases, there exists no re-reconnection at the magnetopause. As a result, reconnected field lines around the magnetopause just wrap around and mix with the magnetosheath flux ropes during the magnetopause reconnection.

3.3. Re-reconnection Between Magnetosheath Flux Ropes and Geomagnetic Dipole Field Lines

We now discuss the interaction between the magnetosheath flux ropes and the magnetopause in cases with an S-N IMF change across the interplanetary TD. Figures 7a–7c display the time evolution of the field line configuration around the magnetopause in case 1 at $t = 60.0\Omega_{i0}^{-1}$, $70.0\Omega_{i0}^{-1}$, and $80.0\Omega_{i0}^{-1}$. A closed dipole field line around the magnetopause is marked by the black line in the figure. The pre-existing magnetopause flux ropes are present by reconnection between the closed geomagnetic dipole field lines and the southward IMF field lines before the arrival of the transmitted TD, as shown at $t = 60.0\Omega_{i0}^{-1}$ and marked as blue field lines in Figure 7a. Meanwhile, the magnetosheah flux rope marked by "F" has already formed, extended in the dawn-dusk direction as denoted by the oranges field lines, with both ends open to the solar wind. At $t = 70.0\Omega_{i0}^{-1}$, the magnetosheath flux rope "F" is going through new reconnection with the geomagnetic dipole field lines at the magnetopause, resulting in the generation of field lines marked by the red and green field lines in Figure 7b. The red reconnected field lines connect from the IMF to the northern hemisphere, and the green field line connect from the southern hemisphere to the IMF. By tracking the red and green field lines around the magnetopause in Figure 7b, it is found that the new reconnection is a re-reconnection with the pre-existing open field lines at the magnetopause, with an X point at $(x,y,z) = (7.9,4.5,3.8)R_E$. The length of the newly reformed magnetopause flux ropes is ~ $11.0R_E$, which is much longer than that of the original magnetopause flux ropes (~ $3R_E$), that is, the blue field lines in Figure 7a, but shorter than that of magnetosheath flux ropes (~ $24.0R_E$, the orange field lines). At $t = 80.0\Omega_{i0}^{-1}$, after the TD passes through the magnetopause, the northward IMF on the sunward side of the TD have reached the magnetopause, which is marked by the yellow field line in Figure 7c. No reconnection structure can be found anymore, except for reconnection between IMF and the dipole field lines above the north cusp.

Let two virtual spacecraft pass through the re-reconnection outflow region in an outbound direction along the black trajectories, marked by "S1" (northward of the re-reconnection X point) and "S2" (southward of the re-reconnection X point) in Figure 7b. To demonstrate the difference between the active reconnection layer and the adjacent flux ropes, the spatial profiles of the magnetic field and plasma quantities along the path of the spacecraft are given in Figure 8, in which the magnetic field and ion bulk velocity are displayed in the LMN coordinates, determined by the minimum variance analysis method, where L is along the antiparallel magnetic field direction, N is along the current layer normal direction, and M is given by $N\times L$. The red bar denotes the locations in the magnetosphere, and the orange bar marks the magnetosheath flux rope "F." The shaded region in the figure represents the magnetopause reconnection current layer. The central

region of the reconnection current layer is denoted by a vertical red dotted line, where $B_L = 0$ and corresponding magnetic field strength has a dip (Figures 8a and 8f). Noted that d_{i0} used in the simulation is $0.1R_E$.

Figure 8a displays the magnetic field magnitude along path "S1" northward of the re-reconnection site, which shows a dip at the location where the B_L component varies from positive value to negative value with a width of $\sim 8d_{i0}$, as shown in Figure 8b. The normal component B_N remains to be a small constant. Outside of the current layer, the flux rope "F" is probed (the orange bar), where the component B_L changes from negative value to positive value, as shown in Figure 8b.

In Figure 8d, there is a northward acceleration of the tangential flow component V_L, to a speed of $\sim 4.0V_{A0}$, due to the existence of an X point southward of the virtual spacecraft location. In addition, the components V_M and V_N have a negative value in the current layer due to the magnetosheath flows above the equator ($z > 0$) and on the duskside ($y > 0$). The corresponding enhancements in the density and the parallel and total ion temperatures are also present at the center of the current layer, as shown in Figures 8c and 8e. On the other hand, along path "S2" southward of the re-reconnection X point, a southward enhancement of the tangential flow component V_L (with a speed of $\sim 3.0V_{A0}$) is present, opposite to V_L along path "S1," indicating an active re-reconnection X point between the two outflow regions. The structure of magnetic field, ion density, and ion temperature are similar to those along path "S1," as shown in Figures 8g–8j. New magnetopause flux ropes are formed by re-reconnection process, denoted by the red and green field lines in Figure 7b.

3.4. About Magnetic Flux Ropes in the Magnetosheath and at the Magnetopause

Overall, when the TD with an S-N field variation crosses the bow shock and then passes through the dayside magnetopause, there are three different reconnection processes, resulting in the generation of different field line configuration of flux ropes. Figure 9 displays the field line configurations before (left column) and after (right column) the three reconnection processes occurring at the magnetopause associated with the initial southward IMF (Figure 9a), in the magnetosheath due to the incoming TD (Figure 9b), and at the magnetopause due to re-reconnection associated with the magnetosheath flux ropes (Figure 9c) in case 1. The symbol "X" denotes the positions of magnetic reconnection. As shown in Figure 9a, the magnetopause reconnection takes place when the initial southward IMF interacts with the magnetopause at the position marked by "X." It is found that four types of flux ropes are formed at the magnetopause before the arrival of the transmitted TD, including the reconnected field lines connected (1) from the IMF to the northern hemisphere (flux rope mentioned in Figure 1), (2) from the southern hemisphere to the IMF, (3) from the IMF to the IMF, and (4) from the southern ionosphere to the northward ionosphere (i.e., closed), as explained by Tan et al. (2012). Figure 9b indicates that, after the TD interacts with the bow shock and enters the magnetosheath, magnetic reconnection is triggered inside the transmitted TD, resulting in the generation of the magnetosheath flux ropes. When the magnetosheath flux ropes interact with the magnetopause, newly reformed magnetopause flux ropes are present, marked as red and black field lines in Figure 9c.

4. Summary and Discussion

In this study, we have used a 3D global hybrid simulation to study the generation of magnetic reconnection in the magnetosheath due to an interplanetary TD with S-N IMF direction change and the subsequent interaction between the magnetosheath flux ropes and the magnetopause. Cases with various field rotation angle $\Delta\Phi$ and half-width w of TD have been investigated. The following main results are obtained:

(1) Since the initial IMF has a southward B_z, magnetopause reconnection occurs before the TDs reach the magnetopause, forming four types of magnetopause flux ropes with length of several R_E
(2) For a fixed $\Delta\Phi = 180°$, magnetosheath flux ropes are formed downstream of both Q-|| and Q-⊥ shocks in the case with $w = 5d_{i0}$. The length of the flux ropes in the dawn-dusk direction is about $6.5R_E$ ($30R_E$) downstream of the Q-|| (Q-⊥) shock, which is longer than that in the magnetopause reconnection. As w increases to $10d_{io}$, magnetic flux ropes are found only in the downstream of the Q-⊥ shock, with a length of $\sim 24R_E$. Under an even thicker initial TD with $w = 30d_{i0}$, magnetosheath reconnection ceases to take place in the magnetosheath

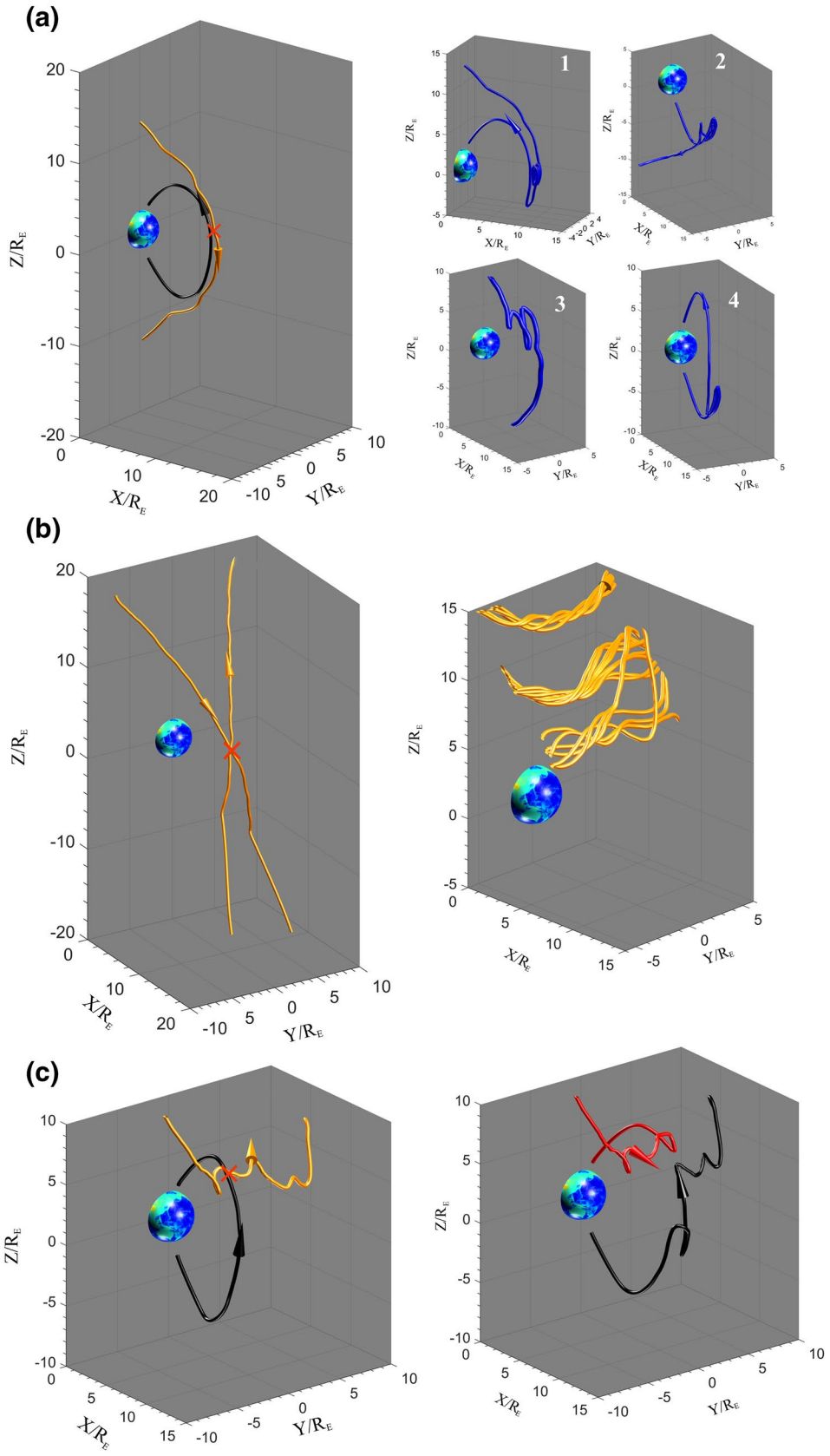
(a)
1
2
3
4
(b)
(c)
Z/R_E
X/R_E
Y/R_E

(3) For a fixed $w = 10d_{i0}$, manetosheath flux ropes are present downstream of the Q-⊥ with a length of $\sim 24R_E$ ($\sim 13R_E$) in case with $\Delta\Phi = 180°(150°)$. As $\Delta\Phi$ decreases to 120°, no magnetic flux rope is found in the entire magnetosheath
(4) When the magnetosheath flux ropes interact with the magnetopause, re-reconnection occurs between the geomagnetic dipole field lines and the magnetosheath flux ropes, forming modified magnetic flux ropes at the magnetopause. The length of the newly reformed flux ropes is larger than that at the magnetopause associated with the initial southward IMF
(5) Under the same conditions of w and $\Delta\Phi$, magnetosheath reconnection occurs less frequently in the present S-N cases than N-S cases (Guo et al., 2018). The transmitted TD convects more quickly in the magnetosheath in the S-N cases than the N-S case due to the existence of the magnetopause reconnection and re-reconnection, and a shorter stay time of TD in the magentosheath in the present cases. There exists re-reconnection at the magnetopause in S-N cases, while no re-reconnection is found in N-S cases

The existence of the four types of magnetopause flux ropes is found in both the present simulation with an oblique IMF and the previous simulation of Tan et al. (2012) with a purely southward IMF (but a finite dipole tilt angle). In a recent MMS spacecraft observation, rope-like structures with magnetospheric energetic electrons and without magnetospheric electrons are found by Russell and Qi (2020). They have highlighted two types of flux ropes at the magnetopause, one type with both ends connected to the magnetosphere while another with both ends connected to the IMF. This finding is consistent with our results of the magnetopause before the arrival of the transmitted TD.

When the transmitted TD crosses the bow shock and moves toward the magnetopause, a thin current sheet forms inside the TD by both the shock compression and the convective compression processes. Reconnection is found to take place in the thin current sheet, forming flux ropes in the magnetosheath. Noted that reconnection in our hybrid simulation is initiated by a current-dependent resistivity. For a relatively thicker TD, it is more difficult to be compressed to a thickness that is thin enough to trigger reconnection in the dayside magnetosheath. In the case with a smaller field rotational angle, the reconnecting magnetic field is also smaller around the reconnection site, corresponding to a smaller current density. As a results, reconnection can be suppressed, especially on the duskside and dawnside of the magnetosheath. Moreover, for the same magnetic field strength, a smaller reconnection rate is found due to the smaller reconnected field flux. Using AMPTE observations, Phan et al. (1994) suggested that low rate of transfer of magnetic flux is present across the magnetopause when the magnetic shear angle is low. As a consequence, reconnection becomes weaker as the rotational angle decreases and the half-width increases in the solar wind TD, resulting in a shorter length of the magnetosheath flux ropes. In the cases with an S-N field variation, the magnetopause reconnection removes the magnetic flux around the magnetopause, which modifies the magnetic field and plasma structures in the magnetosheath, and weakens compression processes. It is found in our simulation that the magnetopause reconnection significantly affects the generation and structure of reconnection/flux ropes inside the TD.

In the global hybrid simulation, an ion inertial length (d_i) larger than the realistic value (in R_E or km) is assumed. As a consequence, one would need to scale back the length when compare the simulation with observations. This is true if the physics and thus the scale lengths are determined by the ion inertial length (d_i) or ion gyroradius (ρ_i). On the other hand, if the length scales are determined by global convection, the length in R_E is realistic. For example, positions of the bow shock and magnetopause in simulation are realistic. Generally speaking, length scales of kinetic processes in the global geometry may be determined by the combination of global and local scales. Similar consideration has been discussed by Guo et al. (2020) when compared the hybrid simulation results with the MMS observations of the magnetopause.

It is also indicated in our simulation that the interaction between the magnetosheath flux ropes and the magnetopause is a complex process. In the present cases with an S-N field variation, the interaction between the magnetosheath flux ropes and the magnetopause is very complicated due to the pre-existence of the magnetopause flux ropes. While re-reconnection is present as the magnetosheath flux ropes arrive

Figure 9. Magnetic field line configuration before and after magnetic reconnection in case 1, (a) at the magnetopause associated with the initial IMF, (b) in the magnetosheath due to the incoming TD, and (c) re-reconnection at the magnetopause associated with the magnetosheath flux ropes. IMF, interplanetary magnetic field; TD, tangential discontinuities.

on the magnetopause reconnection, such re-reconnection is found to take place between the southward segments of the incoming flux ropes and the nearly straight northward part of the magnetopause field lines. Re-reconnection with the helical magnetopause flux ropes, however, is not found because the southward B_z on earthward side of the sheath flux ropes cannot reconnect with the southward B_z on the sunward side of the magnetopause flux ropes. In principle, re-reconnection may also occur in higher latitudes when the magnetosheath flux ropes (which have a sunward B_x on the northward side) move poleward along the magnetopause boundary layer and interact with the pre-existing magnetopause flux ropes (earthward B_x on the southward side), which moves with a relatively slower speed, although it has not been seen in the simulation. Overall, our simulation results provide a systematic study of the interaction between the interplanetary directional TD and the bow shock/dayside magnetopause.

Data Availability Statement

The numerical data used for generating the presented figures are available via https://doi.org/10.6084/m9.figshare.12671135.v1.

Acknowledgments
This work was supported by the grants NASA-80NSSC17K0012 and NASA-NNX17AI47G and DoE grant DEFOA-0001664 to Auburn University, the National Science Foundation of China (Grant 41804160), and China Postdoctoral Science Foundation Funded Project (2018M630198). The computer resources were provided by the National Supercomputer Center of China. The results in this study are generated from our simulation code as described in Section 2.

References

Archer, M. O., Horbury, T. S., & Eastwood, J. P. (2012). Magnetosheath pressure pulses: Generation downstream of the bow shock from solar wind discontinuities. *Journal of Geophysical Research*, *117*, A05228. https://doi.org/10.1029/2011JA017468

Behannon, K. W., Neubauer, F. M., & Barnstorf, H. (1981). Fine-scale characteristics of interplanetary sector boundaries. *Journal of Geophysical Research*, *86*, 3273–3287. https://doi.org/10.1029/JA086iA05p03273

Burlaga, L. F. (1968). Micro-scale structures in the interplanetary medium. *Solar Physics*, *4*, 67.

Burlaga, L. F. (1969). Directional discontinuities in the interplanetary magnetic field. *Solar Physics*, *7*, 54.

Burlaga, L. F. (1971). On the nature and origin of directional discontinuities. *Journal of Geophysical Research*, *76*, 4360.

Burlaga, L. F., Lemaire, J. F., & Turner, J. M. (1977). Interplanetary current sheets at 1 AU. *Journal of Geophysical Research*, *82*, 3191–3200. https://doi.org/10.1029/JA082i022p03191

Burlaga, L. F., & Ness, N. F. (1968). Macro and micro structure of the interplanetary magnetic field. *Canadian Journal of Physics*, *46*, S962.

Crooker, N. U., Eastman, T. E., & Stiles, G. S. (1979). Observations of plasma depletion in the magnetosheath at the dayside magnetopause. *Journal of Geophysical Research*, *84*(A3), 869–874.

Dungey, J. W. (1961). Interplanetary magnetic field and the auroral zones. *Physical Review Letters*, *6*, 47–48. https://doi.org/10.1103/physrevlett.6.47

Eastwood, J. P., Sibeck, D. G., Angelopoulos, V., Phan, T. D., Bale, S. D., McFadden, J. P., et al. (2008). THEMIS observations of a hot flow anomaly: Solar wind, magnetosheath, and ground-based measurements. *Geophysical Research Letters*, *35*, L17S03. https://doi.org/10.1029/2008GL033475

Fu, Z. F., & Lee, L. C. (1985). Simulation of multiple X-line reconnection at the dayside magnetopause. *Geophysical Research Letters*, *12*(5), 291–294. https://doi.org/10.1029/GL012i005p00291

Guo, Z., Lin, Y., Wang, X., & Du, A. (2018). Magnetosheath reconnection before magnetopause reconnection driven by interplanetary tangential discontinuity: A three-dimensional global hybrid simulation with the oblique interplanetary magnetic field. *Journal of Geophysical Research*, *123*, 9169–9186. https://doi.org/10.1029/2018JA025679

Guo, Z., Lin, Y., Wang, X., Vines, S. K., Lee, S. H., & Chen, Y. (2020). Magnetopause reconnection as influenced by the dipole tilt under southward IMF conditions: Hybrid simulation and MMS observation. *Journal of Geophysical Research*, *125*, e2020JA027795. https://doi.org/10.1029/2020JA027795

Hasegawa, H., Wang, J., Dunlop, M. W., Pu, Z. Y., Zhang, Q. H., Lavraud, B., et al. (2010). Evidence for a flux transfer event generated by multiple X-line reconnection at the magnetopause. *Geophysical Research Letters*, *37*, L16101. https://doi.org/10.1029/2010GL044219

Hsu, T.-S., & McPherron, R. L. (2003). Occurrence frequencies of IMF triggered and no triggered substorms. *Journal of Geophysical Research*, *108*(A7), 1307. https://doi.org/10.1029/2002JA009442

Kokubun, S., McPherron, R. L., & Russell, C. T. (1977). Triggering of substorms by solar wind discontinuities. *Journal of Geophysical Research*, *82*(1), 74–86. https://doi.org/10.1029/JA082i001p00074

Le, G., & Russell, C. T. (1992). A study of ULF wave foreshock morphology—I: ULF foreshock boundary. *Planetary and Space Science*, *40*(9), 1203–1213.

Lepping, R. P., & Behannon, K. W. (1986). Magnetic field directional discontinuities: Characteristics between 0.46 and 1.0 AU. *Journal of Geophysical Research*, *91*, 8725–8741.

Lin, Y. (1997). Generation of anomalous flows near the bow shock by its interaction with interplanetary discontinuities. *Journal of Geophysical Research*, *102*(A11), 24265–24281. https://doi.org/10.1029/97JA01989

Lin, Y. (2002). Global hybrid simulation of hot flow anomalies near the bow shock and in the magnetosheath, *Planetary and Space Science*, *50*, 577–591.

Lin, Y. (2003). Global-scale simulation of foreshock structures at the quasi-parallel bow shock. *Journal of Geophysical Research*, *108*(A11), 1390. https://doi.org/10.1029/2003JA009991

Lin, Y., & Wang, X. Y. (2005). Three-dimensional global hybrid simulation of dayside dynamics associated with the quasi-parallel bow shock. *Journal of Geophysical Research*, *110*, A12216. https://doi.org/10.1029/2005JA011243

Liu, Z., Turner, D. L., Angelopoulos, V., & Omidi, N. (2015). THEMIS observations of tangential discontinuity-driven foreshock bubbles. *Geophysical Research Letters*, *42*, 7860–7866. https://doi.org/10.1002/2015GL065842

Lyons, L. R., Blanchard, G. T., Samson, J. C., Lepping, R. P., Yamamoto, T., & Moretto, T. (1997). Coordinated observations demonstrating external substorm triggering. *Journal of Geophysical Research*, *102*, 27039–27051. https://doi.org/10.1029/97JA02639

Maynard, N. C., Sonnerup, B. U. Ö., Siscoe, G. L., Weimer, D. R., Siebert, K. D., Erickson, G. M., et al. (2002). Predictions of magnetosheath merging between IMF field lines of opposite polarity. *Journal of Geophysical Research*, *107*(A12), 1456. https://doi.org/10.1029/2002JA009289

Ness, N. F. (1966). Simultaneous measurements of the interplanetary magnetic field. *Journal of Geophysical Research*, *71*, 3319.

Nishida, A. (1978). *Geomagnetic diagnosis of the magnetosphere*. New York, NY: Springer-Verlag. https://doi.org/10.1007/978-3-642-86825-2

Omidi, N., Eastwood, J. P., & Sibeck, D. G. (2010). Foreshock bubbles and their global magnetospheric impacts. *Journal of Geophysical Research*, *115*, A06204. https://doi.org/10.1029/2009JA014828

Omidi, N., Phan, T., & Sibeck, D. G. (2009). Hybrid simulations of magnetic reconnection initiated in the magnetosheath. *Journal of Geophysical Research*, *114*, A02222. https://doi.org/10.1029/2008JA013647

Omidi, N., Sibeck, D., Blanco-Cano, X., Rojas-Castillo, D., Turner, D., Zhang, H., & Kajdič, P. (2013). Dynamics of the foreshock compressional boundary and its connection to foreshock cavities. *Journal of Geophysical Research*, *118*, 823–831. https://doi.org/10.1002/jgra.50146

Omidi, N., Zhang, H., Chu, C., Sibeck, D., & Turner, D. (2014). Parametric dependencies of spontaneous hot flow anomalies. *Journal of Geophysical Research*, *119*, 9823–9833. https://doi.org/10.1002/2014JA020382

Pang, Y., Lin, Y., Deng, X. H., Wang, X. Y., & Tan, B. (2010). Three-dimensional hybrid simulation of magnetosheath reconnection under northward and southward interplanetary magnetic field. *Journal of Geophysical Research*, *115*, A03203. https://doi.org/10.1029/2009JA014415

Paschmann, G., Baumjohann, W., Sckopke, N., Phan, T.-D., & Lühr, H. (1993). Structure of the dayside magnetopause for low magnetic shear. *Journal of Geophysical Research*, *98*(A8), 13409–13422.

Paschmann, G., Papamastorakis, I., Sckopke, N., Haerendel, G., Bame, S. J., Asbridge, J. R., et al. (1979). Plasma acceleration at the Earth's magnetopause—Evidence for reconnection. *Nature*, *282*, 243–246. https://doi.org/10.1038/282243a0

Phan, T. D., Love, T. E., Gosling, J. T., Paschmann, G., Eastwood, J. P., Oieroset, M., et al. (2011). Triggering of magnetic reconnection in a magnetosheath current sheet due to compression against the magnetopause. *Geophysical Research Letters*, *38*, L17101. https://doi.org/10.1029/2011GL048586

Phan, T.-D., Paschmann, G., Baumjohann, W., Sckopke, N., & Luehr, H. (1994). The magnetosheath region adjacent to the dayside magnetopause: AMPTE/IRM observations. *Journal of Geophysical Research*, *99*, 121–141.

Phan, T. D., Paschmann, G., Twitty, C., Mozer, F. S., Gosling, J. T., Eastwood, J. P., et al. (2007). Evidence for magnetic reconnection initiated in the magnetosheath. *Geophysical Research Letters*, *34*, L14104. https://doi.org/10.1029/2007GL030343

Pudovkin, M. I. (1987). Formation and characteristics of the magnetic barrier in front of the dayside magnetopause. *Geomagnetism and Aeronomy*, *27*, 18–21.

Russell, C., & Qi, Yi. (2020). Flux ropes are born in Pairs: An outcome of interlinked, reconnecting flux tubes. *Geophysical Research Letters*, *47*, e2020GL087620. https://doi.org/10.1029/2020GL087620

Samsonov, A. A., Sibeck, D. G., Dmitrieva, N. P., & Semenov, V. S. (2017). What happens before a southward IMF turning reaches the magnetopause?. *Geophysical Research Letters*, *44*, 9159–9166. https://doi.org/10.1002/2017GL075020

Schwartz, S. J. (1995). Hot flow anomalies near the Earth's bow shock. *Advances in Space Research*, *15*(8/9), 269.

Schwartz, S. J., Paschmann, G., Sckopke, N., Bauer, T. M., Dunlop, M., Fazakerley, A. N., & Thomsen, M. F. (2000). Condition for the formation of hot flow anomalies at Earth's bow shock. *Journal of Geophysical Research*, *105*(12), 12639–12650. https://doi.org/10.1029/1999JA000320

Sibeck, D. G., Borodkova, N. L., Schwartz, S. J., Owen, C. J., Kessel, R., Kokubun, S., et al. (1999). Comprehensive study of the magnetospheric response to a hot flow anomaly. *Journal of Geophysical Research*, *104*, 4577.

Sibeck, D. G., Kudela, K., Lepping, R. P., Lin, R., Nemecek, Z., Nozdrachev, M. N., et al. (2000). Magnetopause motion driven by interplanetary magnetic field variations. *Journal of Geophysical Research*, *105*(25), 155.

Tan, B., Lin, Y., Perez, J. D., & Wang, X. Y. (2012). Global-scale hybrid simulation of cusp precipitating ions associated with magnetopause reconnection under southward IMF. *Journal of Geophysical Research*, *117*, A03217. https://doi.org/10.1029/2011JA016871

Thomsen, M. F., Borovsky, J. E., & Skoug, R. M. (2003). Delivery of cold, dense plasma sheet material into the near-Earth region. *Journal of Geophysical Research*, *108*(A4), 1151. https://doi.org/10.1029/2002JA009544

Thomsen, M. F., Thomas, V. A., Winske, F., Gosling, J. T., Farris, M. H., & Russell, C. T. (1993). Observational test of hot flow anomaly formation by the interaction of a magnetic discontinuity with the bow shock. *Journal of Geophysical Research*, *98*(15), 319.

Wang, R., Nakamura, R., Lu, Q., Baumjohann, W., Ergun, R. E., Burch, J. L., et al. (2017). Simultaneously observed ion- and electron scale quadrants of the reconnection hall magnetic field at magnetopause. *Physical Review Letters*, *118*, 175101. https://doi.org/10.1103/PhysRevLett.118.175101

Wang, S., Zong, Q., & Zhang, H. (2013). Cluster observations of hot flow anomalies with large flow deflections: 1. Velocity deflections. *Journal of Geophysical Research*, *118*, 732–743. https://doi.org/10.1002/jgra.50100